PHYSICAL REVIEW B **89**, 035312 (2014)

Doping Si nanocrystals embedded in SiO_2 with P in the framework of density functional theory

Zhenyi Ni (倪朕伊), Xiaodong Pi (皮孝东),[*] and Deren Yang (杨德仁)
State Key Laboratory of Silicon Materials and Department of Materials Science and Engineering, Zhejiang University, Hangzhou, Zhejiang 310027, China

(Received 6 August 2013; revised manuscript received 20 December 2013; published 24 January 2014)

Despite the popularity of doping silicon nanocrystals (Si NCs) embedded in silicon dioxide (SiO_2), theoretical understanding on the doping of Si NCs has been nearly all directed to hydrogen-passivated freestanding Si NCs. Now we simulate the doping of Si NCs embedded in SiO_2 by constructing Si@SiO_2 models in which Si NCs are completely covered by a thin layer of SiO_2. In the framework of density functional theory, we investigate the locations of P, the binding energies of P, the energy-level schemes, and the radiative recombination for P-doped Si NCs embedded in SiO_2. It is found that a dangling bond at the Si/SiO_2 interface makes a difference for the doping of a Si NC with P. The P doping of Si NCs embedded in SiO_2 vastly differs from that of Si NCs passivated by hydrogen.

DOI: 10.1103/PhysRevB.89.035312 PACS number(s): 73.22.−f, 71.20.Mq, 71.55.Ak, 78.67.Bf

I. INTRODUCTION

Silicon nanocrystals (Si NCs) have been attracting a great deal of attention because of their remarkable electronic and optical properties [1–8]. It is now widely believed that Si NCs should be doped to advance the practical use of Si NCs in all kinds of device structures for photovoltaics [9,10], optoelectronics [11–13], and thermoeletrics [14]. Both theoretical calculation and experimental investigation have been carried out to understand the doping of Si NCs with a variety of dopants [15–19]. Up to now, doping has been experimentally realized for gas-phase-synthesized freestanding Si NCs that are passivated by hydrogen [20–22] and solid-phase-synthesized Si NCs that are embedded in silicon dioxide (SiO_2) [11,23–25]. However, the theoretical understanding of the doping of Si NCs has been nearly all directed toward hydrogen-passivated freestanding Si NCs. It was demonstrated that significant differences in the electronic and optical properties occurred between hydrogen-passivated freestanding Si NCs and those embedded in SiO_2 [26–31]. Therefore, the knowledge gained about hydrogen-passivated freestanding Si NCs should not be directly transferred to those embedded in SiO_2 when doping is concerned.

The prominent feature of Si NCs embedded in SiO_2 is the coverage of Si NCs with SiO_2. This leads to the rationality of simulating the doping of Si NCs embedded in SiO_2 by using a simplified model, in which a Si NC is coated with a thin layer of oxide. Carvalho *et al.* [32] have recently initiated the theoretical investigation on the doping of Si NCs with oxide at the surface. Interesting results that highlighted the difference in doping between hydrogen-passivated Si NCs and those with oxide at the surface were demonstrated. However, their models in which oxide at the surface of Si NCs was simulated by using silanol groups (Si-OH) were hardly realistic. Their models also avoided the effect of the Si/SiO_2 interface on the doping of Si NCs.

In this paper, we construct Si@SiO_2 models in which Si NCs are completely covered by ~ 0.25-nm-thick SiO_2. Despite the rather thin SiO_2 layer at the NC surface, the strain induced by the matrix on Si NCs that are embedded in SiO_2 may be simulated well. In the meantime, defects such as dangling bonds at the Si/SiO_2 interface can be readily considered in our models. Therefore, we believe that the models of Si@SiO_2 should lead to more accurate understanding on the doping of Si NCs that are embedded in SiO_2. In the framework of density functional theory (DFT), we first deal with the doping of Si NCs that are embedded in SiO_2 with P by using the models of Si@SiO_2. The locations of P, the binding energies of P, the energy-level schemes, and the radiative recombination are all investigated for P-doped Si NCs with SiO_2 at the surface. It is found that a dangling bond at the Si/SiO_2 interface makes a difference for the doping of a Si NC with P. We also show that the P doping of Si NCs embedded in SiO_2 vastly differs from that of Si NCs passivated by hydrogen.

II. MODEL AND METHOD

Figure 1 shows the model of an optimized 1.4-nm Si NC that is coated with ~ 0.25-nm-thick SiO_2 with a perfect Si/SiO_2 interface [Si@SiO_2; Fig. 1(a)] or a defective Si/SiO_2 interface at which a Si dangling bond exists [Si@$_{db}SiO_2$; Fig. 1(b)]. The model of Si@SiO_2 is based on a 1.4-nm H-passivated Si NC (Si@H, $Si_{71}H_{84}$), which has been detailed in our previous papers [29,33]. Every H atom in SiH and SiH_3 at the surface of Si@H is initially replaced with an O atom, which is then outwardly bonded to an added Si atom. Only one O atom is inserted between two Si atoms in all neighboring SiH_2 given that the room between neighboring SiH_2 is too small to accommodate both added O and added Si. H passivation at the surface of the resulting structure is finally tuned to render fourfold coordination for all Si atoms. The obtained Si@SiO_2 is in the form of $Si_{123}O_{96}H_{100}$ [Fig. 1(a)].

When a Si dangling bond is considered at the Si/SiO_2 interface, we remove one O atom at the Si/SiO_2 interface. This gives rise to two unsaturated Si atoms. One H atom is used to passivate the unsaturated Si atom that is closer to the surface. The remaining unsaturated Si atom is then associated with $\cdot Si\equiv(SiO_2)$, $\cdot Si\equiv(Si_2O)$, or $\cdot Si\equiv Si_3$ [34–37]. We have compared the formation energies of $\cdot Si\equiv(SiO_2)$, $\cdot Si\equiv(Si_2O)$, and $\cdot Si\equiv Si_3$ by setting the chemical potentials of Si, O, and H at

---

[*] Corresponding author: xdpi@zju.edu.cn

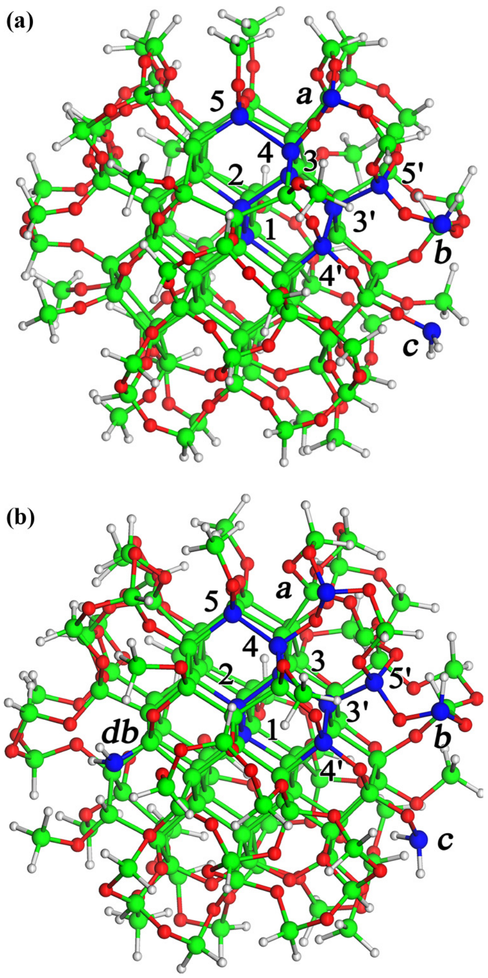

FIG. 1. (Color online) Model of an optimized 1.4-nm Si NC embedded in SiO_2 with (a) a perfect Si/SiO_2 interface ($Si@SiO_2$, $Si_{123}H_{100}O_{96}$) or (b) a defective Si/SiO_2 interface at which a Si dangling bond exists ($Si@_{db}SiO_2$, $Si_{123}H_{101}O_{95}$). Si, H, and O atoms are denoted by green, gray, and red balls, respectively. A substitutional or passivating P atom is indicated by a blue ball. P1, P2, P3 (P3′), P4 (P4′), and P5 (P5′) result from moving a substitutional P atom along the path of 1 → 2 → 3 (3′) → 4 (4′) → 5 (5′). When a P atom replaces a Si atom connected to one, two, or three H atoms at the surface of $Si@SiO_2$, it is denoted as P_a, P_b, or P_c, respectively. As a P atom passivates a Si dangling bond at the Si/SiO_2 interface, it is denoted as P_{db}.

the total energies per atom of bulk Si, O_2, and H_2, respectively. It turns out that the formation energy of $\cdot Si \equiv (Si_2O)$ is the lowest. Therefore, only the most likely formed Si dangling bond that is associated with $\cdot Si \equiv (Si_2O)$ is considered in the current paper [Fig. 1(b)].

Figure 2 shows the strain of a Si-Si bond as a function of the distance between the center of the Si-Si bond and that of $Si@SiO_2$ [Fig. 2(a)] or $Si@_{db}SiO_2$ [Fig. 2(b)]. The strain of a Si-Si bond is obtained by comparing the length of the Si-Si bond with that of a Si-Si bond in bulk Si. For $Si@SiO_2$, on average, both Si-Si bonds near the center and those at the Si/SiO_2 interface are significantly stretched. However, Si-Si bonds at the subinterface and close to the center are either compressed or slightly stretched. This picture is basically similar to what Seino *et al.* [38] have demonstrated for Si NCs embedded in SiO_2. In addition, we find that the band gap of $Si@SiO_2$ is smaller than that of Si@H, consistent with Seino *et al.*'s observation on the oxide-matrix-induced reduction of the NC band gap in their more complicated model [27]. Therefore, our simplified model of $Si@SiO_2$ can fairly simulate the effect that the oxide matrix exerts on Si NCs. For $Si@_{db}SiO_2$, the introduction of a Si dangling bond only moderately alters the strains of Si-Si bonds in the region around the subinterface.

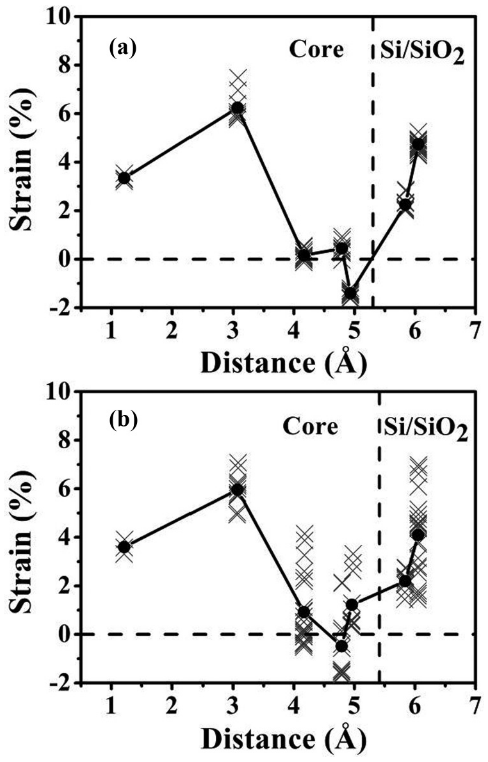

FIG. 2. Change of the strain of a Si-Si bond as a function of the distance between the center of the Si-Si bond and that of (a) $Si@SiO_2$ or (b) $Si@_{db}SiO_2$. The strain of a Si-Si bond is obtained by comparing the length of the Si-Si bond with that of a Si-Si bond in bulk Si (2.34 Å). A cross refers to the strain of a single Si-Si bond. A solid circle refers to the average strain of Si-Si bonds that are with the same distance from the NC center. The solid line is used to guide the eye. The horizontal dashed line that passes through zero indicates that the bond length is the same as that in bulk Si. The vertical dashed line indicates the boundary between the NC core and the Si/SiO_2 interface region.

A variety of substitutional locations of P are investigated for the doping of $Si@SiO_2$ and $Si@_{db}SiO_2$ with P [Figs. 1(a) and 1(b)]. P1, P2, P3 (P3′), P4 (P4′), and P5 (P5′) result from moving a substitutional P atom along the path of 1 → 2 → 3 (3′) → 4 (4′) → 5 (5′). When a P atom replaces a Si atom connected to one, two, or three H atoms at the surface of $Si@SiO_2$ or $Si@_{db}SiO_2$, it is denoted as P_a, P_b, or P_c, respectively. P_a, P_b, and P_c are passivated by zero, one, and two H atoms, respectively. As a P atom passivates a Si dangling bond at the Si/SiO_2 interface, it is denoted as P_{db}.

The optimization of structures and the calculation of total energies are performed at 0 K by using the all-electron DFT modeling package DMol3 [29,39,40]. The Becke-Lee-Yang-Parr correlation exchange functional at the generalized gradient approximation level is used. Double numerical basis sets augmented with p-polarization functions are employed as the atomic orbital basis functions. To ensure accurate calculation, a high self-consistent filed convergence threshold of 10^{-6} is employed. The maximum forces on all of the atoms in the optimized structures are less than 0.002 Ha/Å. For study on the optical absorption of Si NCs, the time-dependent density functional theory (TD-DFT) with adiabatic local density approximation (ALDA) implemented in the package of DMol3 is employed. The first 80 allowed transitions are considered for each NC. Lorentzian broadening with a full width at half maximum of 20 nm is carried out to generate each absorption spectrum.

When a Si NC is excited, an electron in the highest occupied molecular orbital (HOMO) transits to the lowest unoccupied molecular orbital (LUMO), leaving a hole in the HOMO. After the HOMO-LUMO transition, structural and electronic optimization are performed to obtain the relaxed geometry of the Si NC at the excited state. For Si NCs at both the ground state and excited state, the HOMO-LUMO gaps are readily calculated once the Si NC optimization is finished. For a Si NC larger than 1 nm, the excitation energy (E_{ex}) and emission energy (E_{em}) of the Si NC are similar to the HOMO-LUMO gaps at the ground state and excited state, respectively [41–43]. Such similarities are adopted to determine the E_{ex} and E_{em} of a Si NC in this paper. The values of E_{ex} and E_{em} are usually underestimated by $\sim 1-2$ eV in DFT calculations [44,45]. However, the relative order between the values of E_{ex} or between those of E_{em} is not seriously affected by the underestimation [44]. Meaningful results on the excited state of a Si NC can also be obtained with DFT [41,46,47], although the exited state is often investigated in the framework of TD-DFT [48–52] by using the Pseudopotential Algorithm for Real-Space Electronic Structure Calculations (PARSEC) code [42] and the Open Repository Case Application (ORCA) programming interface [53]. Radiative recombination rates for Si NCs are numerically calculated in momentum space by using Fermi's golden rule [54–56]:

$$R_{i,f} = \left(\frac{16\pi^2 n\theta^2}{3\hbar^2 m^2 c^2}\right) E_{i,f} |\langle\phi_i|\hat{p}|\phi_f\rangle|^2. \tag{1}$$

Here, ϕ_i and ϕ_f are the wave functions of the HOMO and LUMO of a Si NC at the excited state, respectively; $E_{i,f}$ is the transition energy between state i and state f; m is the electron rest mass; e is the electronic charge; n is the refractive index of the Si NC, which is 2.34 for the NC size of 1.4 nm [57]; c is the velocity of light; and $\hat{p}$ is the momentum operator. In this paper, only non-phonon-assisted electronic transitions are considered in the calculation of radiative recombination rates [2]. The matrices of the HOMO/LUMO wave functions are obtained by discretely sampling three-dimensional space with a grid space of 0.2 Å.

III. RESULTS AND DISCUSSION

A. Formation energy

We have calculated the formation energy (E_f) of a P atom in Si@$\mathrm{SiO_2}$ or Si@$_{db}\mathrm{SiO_2}$ by using [58]

$$E_f = E(\mathrm{Si}_{x'}\mathrm{O}_{y'}\mathrm{H}_{z'}\mathrm{P}) - E(\mathrm{Si}_x\mathrm{O}_y\mathrm{H}_z) - \mu_\mathrm{P} - (x'-x)\mu_\mathrm{Si} - (y'-y)\mu_\mathrm{O} - (z'-z)\mu_\mathrm{H}. \tag{2}$$

Here, $E(\mathrm{Si}_x\mathrm{O}_y\mathrm{H}_z)$ and $E(\mathrm{Si}_{x'}\mathrm{O}_{y'}\mathrm{H}_{z'}\mathrm{P})$ are the total energy of Si@$\mathrm{SiO_2}$ or Si@$_{db}\mathrm{SiO_2}$ before and after the incorporation of a P atom, respectively; x (x'), y (y'), and z (z') are the numbers of Si, O, and H atoms, respectively; and μ_Si, μ_O, μ_H, and μ_P are the chemical potentials of Si, O, H, and P, respectively. The total energies of atomic Si, O, H, and P in bulk Si, oxygen gas, hydrogen gas, and orthorhombic black phosphorus are used for μ_Si, μ_O, μ_H, and μ_P, respectively [54,59]. Although these choices of chemical potentials may not exactly reflect the doping process of Si NCs embedded in $\mathrm{SiO_2}$, the relative order of E_f for P in all kinds of configurations is not affected given the linear relationship between E_f and each chemical potential. Figure 3 shows the values of E_f as a substitutional P atom moves from the center to the surface for Si@$\mathrm{SiO_2}$ [Fig. 3(a)] and Si@$_{db}\mathrm{SiO_2}$ [Fig. 3(b)]. It is clear that the values of E_f for P at the Si/$\mathrm{SiO_2}$ interface and the surface of Si@$\mathrm{SiO_2}$ (i.e., the locations of 4 (4′), 5 (5′), a, b, and c) are larger than those for P in the NC core [Fig. 3(a)]. Si atoms at the Si/$\mathrm{SiO_2}$ interface and the surface of Si@$\mathrm{SiO_2}$ are all associated with O. It is the strong bonding between Si and O that raises the barrier for the substitution of P to Si [60]. Si atoms in the locations of 5′ and a are bonded to three O atoms. The largest number

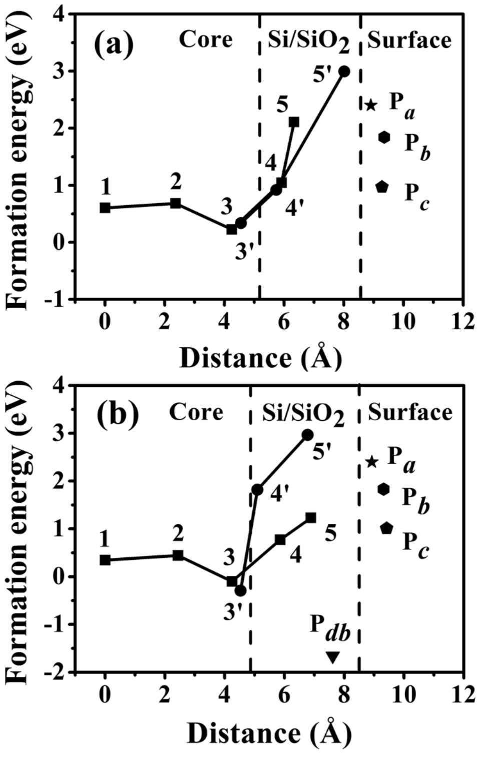

FIG. 3. Formation energy of P in (a) Si@$\mathrm{SiO_2}$ or (b) Si@$_{db}\mathrm{SiO_2}$ as P substitutionally moves from the center to the surface.

(three) of O atoms that are bonded to a Si atom leads to the highest values of E_f for P5′ and P_a in this paper. The value of E_f for P3 (P3′) at the subinterface is the lowest (0.2 ∼ 0.3 eV), indicating that P is the most likely doped to the subinterface in terms of thermodynamics. This is similar to the distribution of P in both oxidized Si nanowires [61,62] and oxidized bulk Si [63,64], indicating that the curvature of the Si/SiO$_2$ interface does not affect the distribution of P in oxidized Si. On one hand, attractive interaction between a P atom and electronegative oxygen atoms causes the P atom to be favorably positioned toward SiO$_2$ [32]. On the other hand, strong bonding between Si and O may retard the replacement of Si with P in SiO$_2$ [60]. Hence, P is the most likely incorporated into the subinterface region of all types of Si/SiO$_2$. The fact that the P atom is the most likely incorporated into the subinterface region of Si@SiO$_2$ is in contrast to the doping of Si@H with P, where P preferentially resides at the surface of Si@H [54]. In addition, P prefers the core of a Si NC to the oxide surrounding the NC, given the much lower values of E_f for P in the NC core [Fig. 3(a)]. Therefore, the doping of Si NCs embedded in SiO$_2$ can be validated.

The dependence of E_f on the location of P for Si@$_{db}$SiO$_2$ is essentially similar to that for Si@SiO$_2$ except that the E_f of P_{db} is the lowest (−1.66 eV). Mimura *et al.* [25] assumed that P should passivate defects such as Si dangling bonds at the Si/SiO$_2$ interface when Si NCs embedded in SiO$_2$ were very lightly doped with P. Our result is basically consistent with their assumption. It is seen that a Si dangling bond at the Si/SiO$_2$ interface hardly affects the values of E_f for P at the surface of Si@$_{db}$SiO$_2$ (the relative change of E_f is ∼0%–4%). However, the values of E_f for P in the NC core or at the Si/SiO$_2$ interface are all reduced as a Si dangling bond exists at the Si/SiO$_2$ interface, except for the configuration of P4′. This means that defects such as Si dangling bonds at the Si/SiO$_2$ interface may facilitate the incorporation of P for Si NCs embedded in SiO$_2$. The exceptional case of P4′ is because in the optimized structure of Si@SiO$_2$, a P4′ atom is only bonded to an O atom and two Si atoms, leaving a dangling bond of an O atom. However, this structural distortion does not occur in the optimized structure of Si@$_{db}$SiO$_2$.

B. Electronic properties

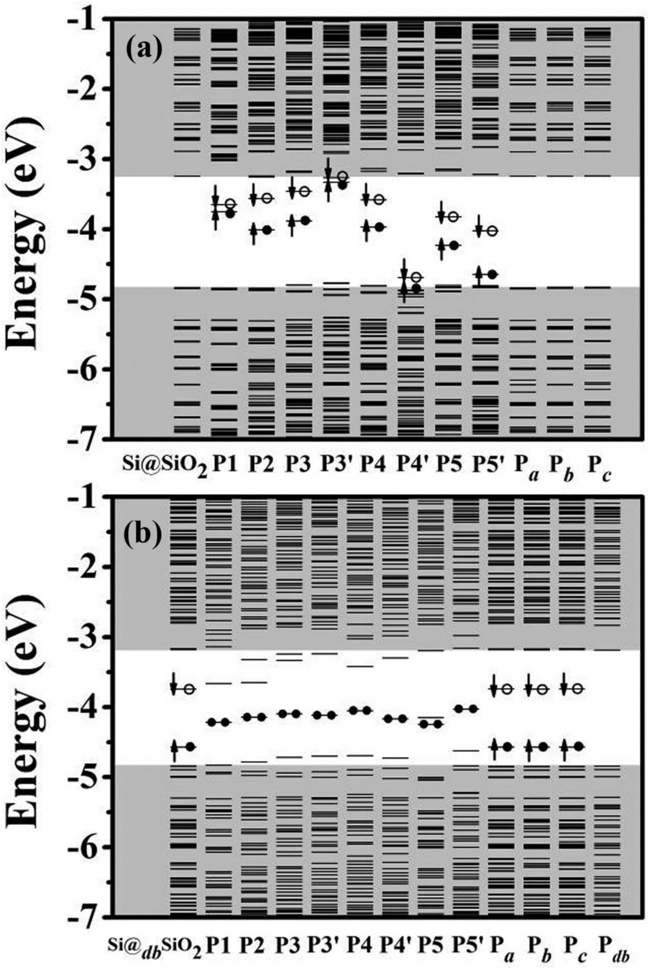

FIG. 4. Energy-level diagrams for undoped and P-doped (a) Si@SiO$_2$ or (b) Si@$_{db}$SiO$_2$ at the ground state. Filled circles indicate that energy levels are occupied by electrons, whereas empty circles indicate that they are unoccupied by electrons. Spin-up states of P-induced defect energy levels are indicated by up arrows, whereas spin-down states are indicated by down arrows.

The energy-level diagrams for undoped and P-doped Si@SiO$_2$ or Si@$_{db}$SiO$_2$ at the ground state are shown in Fig. 4. For Si@SiO$_2$, deep energy levels are introduced in the band gap when P is in the configurations of P1, P2, P3 (P3′), P4 (P4′), and P5 (P5′). This is mainly due to the P-doping-induced odd number of electrons in a NC. Traditionally speaking, the incorporation of P in these configurations is no more doping. Doping should lead to rather shallow energy levels in the band gap, as occurs to bulk Si. Nevertheless, for convenience, we continue to call the incorporation of P in these configurations into Si NCs doping. We find that the electron wave functions of the HOMO and LUMO are mainly localized at P1, P2, P3 (P3′), P4, or P5 (P5′) (in these cases, the HOMO and LUMO actually refer to the deep energy levels). This is representatively shown for Si@SiO$_2$ doped with P3 in Fig. 5. It is these localizations that contribute to the deep energy levels. For the configuration of P4′ in Si@SiO$_2$, the aforementioned exceptional structural distortion causes the electron wave function of the HOMO to be delocalized in the whole NC and that of the LUMO to be localized at the O dangling bond. For undoped Si@SiO$_2$, the electron wave functions of the HOMO and LUMO are all delocalized in the whole NC (Fig. 5). It is seen that for P-doping-induced states there is spin splitting, which is associated with the polarizability of bonds. Clearly, the polarizability of bonds may be influenced by bond length. When P is doped in the configuration of P1 or P3′, a rather small change (< 1%) of bond length occurs, giving rise to small spin splitting. However, there are significant changes (6% ∼ 35%) of bond length when P is doped in the configurations of P2, P3, P4 (P4′), and P5 (P5′). Therefore, the spin splitting of the states induced by P in these configurations is large.

Figure 4 shows that the band gap of undoped Si@$_{db}$SiO$_2$ is slightly larger than that of undoped Si@SiO$_2$ (1.66 vs 1.59 eV). In the meantime, the electron wave functions of the HOMO and LUMO of Si@$_{db}$SiO$_2$ are mainly localized at the dangling bond (Fig. 5). When a P atom passivates the dangling bond with the configuration of P_{db}, the electron wave functions of

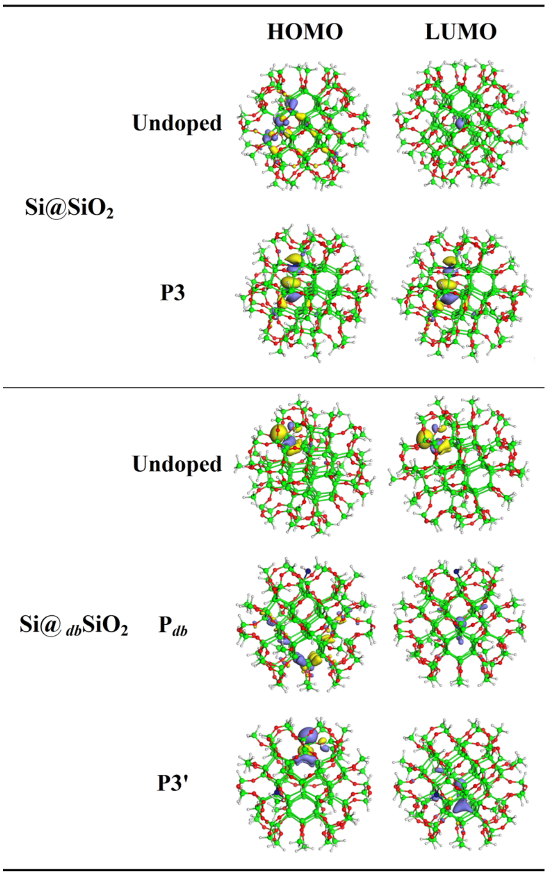

FIG. 5. (Color online) Distribution of the electron wave functions of the HOMO and LUMO for P3-doped $Si@SiO_2$ and P_{db} or P3′-doped $Si@_{db}SiO_2$. Those for the undoped NCs are also shown for comparison.

the HOMO and LUMO are delocalized in the whole structure (Fig. 5), eliminating deep energy levels in the band gap (Fig. 4). This is because there remain no unpaired electrons after the passivation of the Si dangling bond by P_{db}. We should note that the incorporation of P_{db} is not the doping that is traditionally carried out in bulk Si, because P_{db} does not introduce energy levels in the band gap at all. However, for $Si@_{db}SiO_2$ doped with P in the configurations of P1, P2, P3 (P3′), P4 (P4′), and P5 (P5′), deep energy levels remain. The electron wave functions of the HOMO are localized on the dangling bond, while those of the LUMO are localized on P (the case for P3′ is representatively shown in Fig. 5). The single electron of a P atom in the configuration of P1, P2, P3 (P3′), P4 (P4′), or P5 (P5′) is transferred to form an electron pair with that of the Si dangling bond. The electron pair occupies the HOMO with opposite spins, consistent with the Pauli's exclusion principle. Similar to what happens to $Si@SiO_2$, the incorporation of P in these configurations is not traditional doping, because they do not lead to any shallow energy levels in the band gap. The incorporation of P_a, P_b, or P_c hardly changes the energy-level scheme of $Si@SiO_2$ or $Si@_{db}SiO_2$ (Fig. 4), because P_a, P_b, or P_c is in threefold coordination at the surface without introducing a single electron. The absence of energy levels induced by P_a, P_b, and P_c indicates that P_a, P_b, and P_c are actually not dopants if we speak of traditional doping.

TABLE I. Affinity energy (E_a) of undoped Si@H, $Si@SiO_2$, or $Si@_{db}SiO_2$, and ionization energy (E_i) and binding energy (E_b) of singularly and doubly P-doped Si@H, $Si@SiO_2$, or $Si@_{db}SiO_2$.

	E_a (eV)	P	E_i (eV)	E_b (eV)
Si@H	1.65	P_a	6.37	4.72
		P_a- P_b	6.40	4.75
$Si@SiO_2$	2.54	P3	4.41	1.86
		P3-P3′	5.39	2.85
$Si@_{db}SiO_2$	3.23	P_{db}	5.64	2.41
		P_{db}-P3′	4.10	0.87

We have calculated the ionization energy E_i of P-doped $Si@SiO_2$ or $Si@_{db}SiO_2$ and the affinity energy E_a of undoped $Si@SiO_2$ or $Si@_{db}SiO_2$ by using

$$E_i = E_d\,(n-1) - E_d\,(n) \tag{3}$$

and

$$E_a = E_u\,(n) - E_u\,(n+1)\,, \tag{4}$$

where E_d is the total energy of the n or $n-1$ electrons system for doped $Si@SiO_2$ or $Si@_{db}SiO_2$ at 0 K and E_u is similar for the undoped version. The binding energy E_b is defined as the energy needed to transfer an electron from P-doped $Si@SiO_2$ ($Si@_{db}SiO_2$) to undoped $Si@SiO_2$ ($Si@_{db}SiO_2$):

$$E_b = E_i - E_a. \tag{5}$$

The definition of E_b here is different from that for a bulk system [58,65], where E_b is the difference between the dopant-induced energy level and the conduction band minimum or valence band maximum.

Table I shows E_a, E_i, and E_b of P-doped $Si@SiO_2$ or $Si@_{db}SiO_2$. E_a, E_i, and E_b of P-doped Si@H are also listed for comparison [54]. The P configuration with the lowest E_f is first separately considered. Then the P configuration with the second-lowest E_f is considered, together with that with the lowest E_f to exemplarily study the synergic effect of P in different configurations. We see that the value of E_a for $Si@SiO_2$ is larger than that for Si@H. This should be due to the large electronegativity of O atoms in $Si@SiO_2$. However, the value of E_i for P-doped $Si@SiO_2$ is smaller than that for P-doped Si@H. Therefore, the value of E_b for $Si@SiO_2$ is significantly smaller than that for Si@H. The current result is different from Carvalho *et al.*'s, which shows larger E_b for OH-passivated Si NCs compared with Si@H [32]. Such a difference signifies that our understanding on the doping of Si NCs critically depends on simulation models. The value of E_b for $Si@_{db}SiO_2$ may be further reduced because of the dangling-bond-induced increase of E_a. It is clear that for P-doped Si@H, E_b is too large to enable the transport of electrons between NCs. When an odd number of electrons are introduced by P (e.g., P3-doped $Si@SiO_2$ or P_{db}-P3′ co-doped $Si@_{db}SiO_2$), unpaired electrons lead to the decrease of E_i. Hence, E_b may be rather small, indicating a lower threshold of energy for the transport of electrons between two $Si@SiO_2$ ($Si@_{db}SiO_2$) entities. Please note that oxide-matrix-induced energy barriers are not taken into account here.

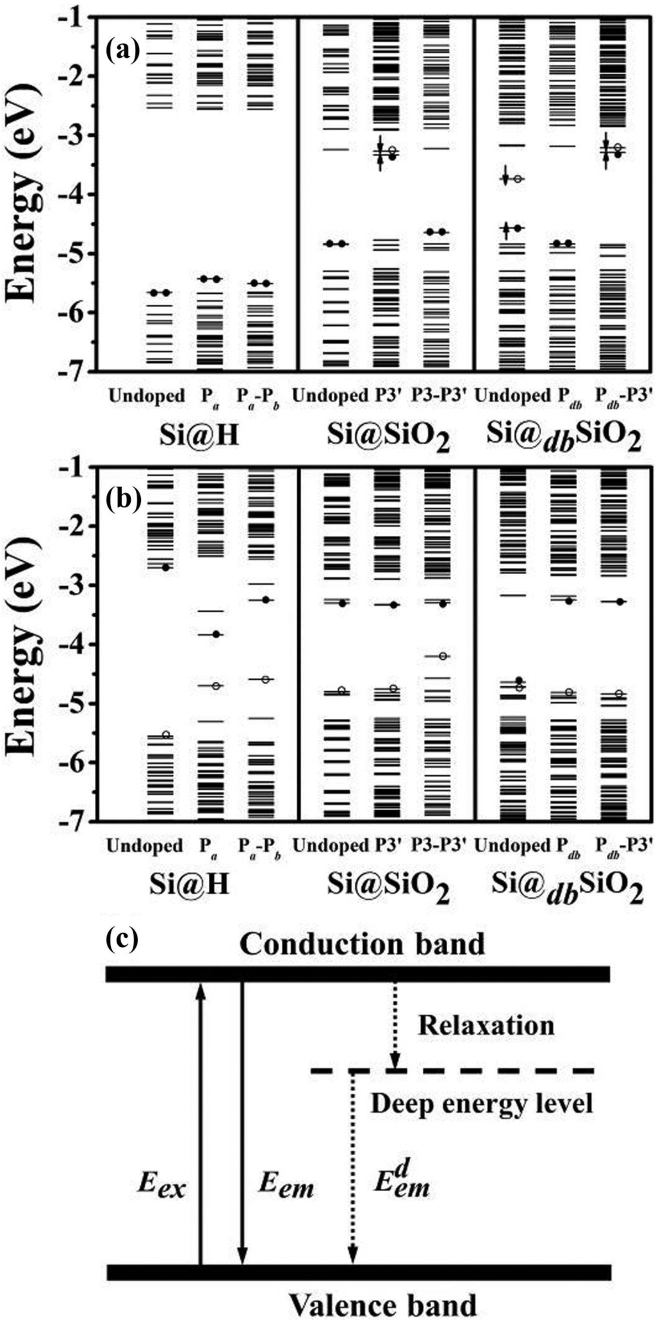

FIG. 6. Energy-level diagrams of undoped, singularly, and doubly P-doped Si@H, Si@SiO$_2$ or Si@$_{db}$SiO$_2$ at the (a) ground state and (b) excited state. For a Si NC with deep energy levels (Si@SiO$_2$ doped with P3′, undoped Si@$_{db}$SiO$_2$, or Si@$_{db}$SiO$_2$ doped with P$_{db}$-P3′), an excited electron has already relaxed to the deep energy level for the excited state. Filled circles indicate that energy levels are occupied by electrons, whereas empty circles indicate that they are unoccupied by electrons. Spin-up (spin-down) states of P-induced defect energy levels are indicated by up (down) arrows. (c) The excitation, relaxation, and radiative recombination of an electron in a Si NC.

TABLE II. Excitation energy (E_{ex}), emission energy (E_{em}), and radiative recombination rate (R) of undoped, singularly, and doubly P-doped Si@H, Si@SiO$_2$, or Si@$_{db}$SiO$_2$. The superscript letter d indicates a value that corresponds to recombination related to a deep energy level.

		E_{ex} (eV)	E_{em} (eV)	R (10^6 s^{-1})
	Undoped	3.13	2.85	1.3
Si@H	P$_a$	2.87	0.86	114.6
	P$_a$-P$_b$	2.95	1.34	27.1
	Undoped	1.59	1.50	1.5
Si@SiO$_2$	P3′	1.88	1.43^d	0.2^d
	P3-P3′	1.42	0.91	271.0
	Undoped	1.66	0.07^d	0.97^d
Si@$_{db}$SiO$_2$	P$_{db}$	1.66	1.57	39.4
	P$_{db}$-P3′	2.02	1.56^d	29.5^d

C. Optical properties

We now move to investigate the optical excitation and emission of P-doped Si@SiO$_2$ or Si@$_{db}$SiO$_2$. For comparison, P-doped Si@H is also considered. Here, only P atoms in the most likely configurations are taken into account. Figure 6 shows the energy-level diagrams of undoped, singularly P-doped, and doubly P-doped Si@H, Si@SiO$_2$, or Si@$_{db}$SiO$_2$ at the ground state [Fig. 6(a)] and excited state [Fig. 6(b)]. The excitation energy (E_{ex}) here corresponds to the transition from the top of the valence band to the bottom of the conduction band. When there are no deep energy levels in the band gap, the emission energy (E_{em}) corresponds to the transition from the bottom of the conduction band to the top of the valence band. However, an excited electron may readily relax to the deep energy levels if there are deep energy levels in the band gap [1,66]. The subsequent transition from the deep energy levels to the top of the valence band may also lead to radiative recombination with the emission energy of E_{em}^d. This has been schematically shown in Fig. 6(c). The excitation energy, emission energy, and radiative recombination rate (R) for each of these structures are listed in Table II. The optical absorption spectra of undoped, singularly, and doubly P-doped Si@H, Si@SiO$_2$, and Si@$_{db}$SiO$_2$ are shown in Figs. 7(a)–7(c).

For Si@H at the ground state, neither P$_a$ nor P$_a$-P$_b$ introduces deep energy levels in the band gap. But they slightly narrow the band gap, leading to the reduction of E_{ex}. This is consistent with the red shift of the absorption when P is doped as P$_a$ or P$_a$-P$_b$ [Fig. 7(a)]. At the excited state, both P$_a$ and P$_a$-P$_b$ significantly reduce the band gap, leading to the large red shift of E_{em}. In the meantime, the P doping causes R to increase by one to two orders of magnitude.

For singularly P-doped Si@SiO$_2$, deep energy levels are introduced in the band gap. Excitation related to these deep energy levels gives rise to small absorption peaks in the low-energy region of the absorption spectrum [Fig. 7(b)], although the E_{ex} blueshifts (1.88 vs 1.59 eV). The E_{em}^d related to the P-induced deep energy level slightly redshifts compared with the E_{em} for undoped Si@SiO$_2$ (1.43 vs 1.50 eV). It is interesting that R for the radiative recombination related to the P-induced deep energy level is smaller than that related to the band-to-band transition of undoped Si@SiO$_2$ by about one order of magnitude (0.2×10^{-6} vs 1.5×10^{-6} s^{-1}). When Si@SiO$_2$ is doped with two P atoms, no deep energy levels exist in the band gap because of the avoidance of an odd electron number. However, the E_{ex} is reduced, consistent with the red shift of the

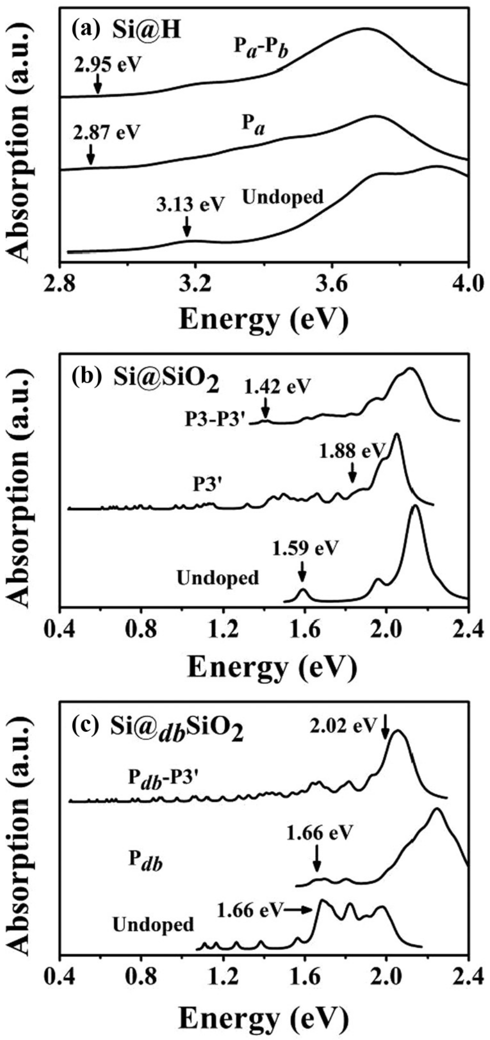

FIG. 7. Optical absorption spectra of undoped, singularly, and doubly P-doped (a) Si@H, (b) Si@SiO$_2$, or (c) Si@$_{db}$SiO$_2$. The calculations are performed in the framework of TD-DFT with the ALDA exchange-correlation functional. The first 80 allowed transitions are considered for each NC. Lorentzian broadening with a full width at half maximum of 20 nm is carried out to generate each absorption spectrum. The excitation energy (E_{ex}) that corresponds to the transition from the top of the valence band to the bottom of the conduction band is indicated by the arrow.

absorption [Fig. 7(b)]. We also find that the E_{em} is reduced. The R for the band-to-band transition is enhanced by more than 200 times.

For undoped Si@$_{db}$SiO$_2$, the dangling bond introduces deep energy levels in the band gap, similar to P3 in Si@SiO$_2$. The E_{ex} of Si@$_{db}$SiO$_2$ is only slightly larger than that of Si@SiO$_2$. However, absorption with energies lower than the E_{ex} is prominent for Si@$_{db}$SiO$_2$ [Fig. 7(c)]. The low-energy absorption is associated with excitation related to deep energy levels that are introduced by the dangling bond. The state related to the dangling bond is radiative, although the corresponding E_{em} is rather small. Once the dangling bond is passivated by a P atom, the electronic structure of Si@$_{db}$SiO$_2$ is basically similar to that of undoped Si@SiO$_2$. Therefore, the E_{ex}, E_{em}, and optical absorption spectrum for Si@$_{db}$SiO$_2$ doped with P$_{db}$ are similar to those for undoped Si@SiO$_2$. However, R for Si@$_{db}$SiO$_2$ doped with P$_{db}$ is ~30 times larger than that for undoped Si@SiO$_2$. If a second P atom (e.g., P3′) is incorporated in addition to P_{db}, an odd electron number appears, leading to deep energy levels in the band gap. The resulting electronic structure is similar to that of Si@SiO$_2$ doped with a single P atom (e.g., P3′) and hence leads to similar optical properties.

In the current paper, P-induced deep energy levels are radiative, leading to light emission with energies smaller than the band gaps. This is consistent with Delerue *et al.*'s paper [55], which has shown that for rather small Si NCs (i.e., band gaps larger than ~ 2.2 eV) defects such as dangling bonds can be centers for radiative recombination. Now we further demonstrate that the band gap of a Si NC may be narrowed without the introduction of deep energy levels if an even electron number is introduced by the doping of multiple P atoms, leading to the red shift of the light emission from the Si NC. Therefore, the doping of P can be an effective means to tune the light emission from Si NCs, especially for the case of coaxing subband luminescence from Si NCs.

IV. CONCLUSIONS

We have studied the P doping of a 1.4-nm Si NC embedded in SiO$_2$ (Si@SiO$_2$ and Si@$_{db}$SiO$_2$). In contrast to the doping of Si@H with P, P is the most likely incorporated into the subinterface of Si@SiO$_2$. However, for Si@$_{db}$SiO$_2$ with a dangling bond at the Si/SiO$_2$ interface, a P atom prefers passivating the dangling bond. The dangling bond at the Si/SiO$_2$ interface may lower the formation energy of P inside the NC core. SiO$_2$ at the NC surface helps reduce the binding energy of P in Si NCs. The reduction of the binding energy of P may be further enhanced as an odd electron number is introduced by P doping.

For singularly P-doped Si@SiO$_2$, the P-induced state may cause the E_{ex} and E_{em} to blueshift and redshift, respectively. When two P atoms coexist in Si@SiO$_2$, no deep energy levels are introduced in the band gap. The E_{ex} and E_{em} are significantly reduced. But the radiative recombination rate enormously increases.

For Si@$_{db}$SiO$_2$, the passivation of the dangling bond with P (P_{db}) leads to the E_{ex} and E_{em} that are similar to those for Si@SiO$_2$. But the radiative recombination is enhanced compared to that for Si@SiO$_2$. When a second P atom is incorporated into Si@$_{db}$SiO$_2$ in addition to P_{db}, dopant-induced deep energy levels appear. This gives rise to the similarity to singularly P-doped Si@SiO$_2$.

We have also considered a smaller (1.2 nm) Si NC with SiO$_2$ at the NC surface. The preferential distribution of P in Si@SiO$_2$ or Si@$_{db}$SiO$_2$ for the NC size of 1.2 nm is similar to that for the NC size of 1.4 nm. The E_{ex} of P-doped Si@SiO$_2$ or Si@$_{db}$SiO$_2$ redshifts for the NC size of 1.2 nm. This is partially different from that for the NC size of 1.4 nm, in which the E_{ex} blueshifts for singularly P-doped Si@SiO$_2$ or doubly P-doped Si@$_{db}$SiO$_2$. The difference in the doping-induced variation of E_{ex} between the NC sizes of 1.2 and 1.4 nm may originate from P-doping-induced structural distortion at the ground state. For instance, for singularly P-doped Si@SiO$_2$ with the NC size of 1.2 nm, the difference between the longest and the shortest Si-P bonds is ∼ 0.21 Å, which is four times larger than that for singularly P-doped Si@SiO$_2$ with the NC size of 1.4 nm. The variation of the emission energy for P-doped Si@SiO$_2$ or Si@$_{db}$SiO$_2$ with the NC size of 1.2 nm is similar to that with the NC size of 1.4 nm, except that the emission energy of P-doped Si@SiO$_2$ more significantly redshifts for the NC size of 1.2 nm. The states related to P atoms are radiative for both the NC sizes. The R for P-doped Si@SiO$_2$ or Si@$_{db}$SiO$_2$ all significantly decreases for the NC size of 1.2 nm, in contrast to that for the NC size of 1.4 nm. The aforementioned comparisons indicate that the NC size also plays a role for a Si NC at the excited state. This is consistent with our finding that excitation-induced structural distortion for 1.2-nm Si@SiO$_2$ is more serious than that for 1.4-nm Si@SiO$_2$. Since the structural distortion becomes negligible when the NC size is ≥1.4 nm [41,67], the current findings for the 1.4-nm Si NC may only be extended to larger Si NCs.

ACKNOWLEDGMENTS

Prof. Jun Xu at Nanjing University is thanked for discussion during this work. Shanghai Supercomputer Center is acknowledged for providing computation resources. This paper is mainly supported by the National Basic Research Program of China (Grant No. 2013CB632101) and the National Natural Science Foundation of China for excellent young researchers (Grant No. 61222404). Partial support from the research and development program of the Ministry of Education of China (Grant No. 62501040202) is acknowledged.

[1] L. Pavesi, L. D. Negro, C. Mazzoleni, G. Franzò, and F. Priolo, Nature **408**, 440 (2000).

[2] D. Kovalev, H. Heckler, M. Ben-Chorin, G. Polisski, M. Schwartzkopff, and F. Koch, Phys. Rev. Lett. **81**, 2803 (1998).

[3] A. G. Cullis, L. T. Canham, and P. D. J. Calcott, Appl. Phys. Rev. **82**, 909 (1997).

[4] Y. Chao, L. Šiller, S. Krishnamurthy, P. R. Coxon, U. Bangert, M. Gass, L. Kjeldgaard, S. N. Patole, L. H. Lie, N. O'Farrell, T. A. Alsop, A. Houlton, and B. R. Horrocks, Nat. Nanotechnol. **2**, 486 (2007).

[5] E. G. Barbagiovanni, D. J. Lockwood, P. J. Simpson, and L. V. Goncharova, J. Appl. Phys. **111**, 034307 (2012).

[6] X. D. Pi, R. W. Liptak, J. Deneen Nowak, N. P. Wells, C. B. Carter, S. A. Campbell, and U. Kortshagen, Nanotechnology **19**, 245603 (2008).

[7] Z. Deng, X. D. Pi, J. J. Zhao, and D. R. Yang, J. Mater. Sci. Technol. **29**, 221 (2013).

[8] G. G. Qin, G. Z. Ran, K. Sun, and H. J. Xu, J. Nanosci. Nanotechnol. **10**, 1584 (2010).

[9] X. J. Hao, E. C. Cho, C. Flynn, Y. S. Shen, G. Conibeer, and M. A. Green, Nanotechnology **19**, 424019 (2008).

[10] I. Perez-Wurfl, X. Hao, A. Gentle, D.-H. Kim, G. Conibeer, and M. A. Green, Appl. Phys. Lett. **95**, 153506 (2009).

[11] M. Fujii, A. Mimura, S. Hayashi, and K. Yamamoto, Appl. Phys. Lett. **75**, 184 (1999).

[12] K. Fujio, M. Fujii, K. Sumida, S. Hayashi, M. Fujisawa, and H. Ohta, Appl. Phys. Lett. **93**, 021920 (2008).

[13] M. Fujii, Y. Yamaguchi, Y. Takase, K. Ninomiya, and S. Hayashi, Appl. Phys. Lett. **85**, 1158 (2004).

[14] R. Lechner, H. Wiggers, A. Ebbers, J. Steiger, M. S. Brandt, and M. Stutzmann, Phys. Status Solidi RRL **1**, 262 (2007).

[15] R. N. Pereira, A. J. Almeida, A. R. Stegner, M. S. Brandt, and H. Wiggers, Phys. Rev. Lett. **108**, 126806 (2012).

[16] M. Perego, C. Bonafos, and M. Fanciulli, Nanotechnology **21**, 025602 (2010).

[17] K. Sato, N. Fukata, and K. Hirakuri, Appl. Phys. Lett. **94**, 161902 (2009).

[18] S. A. Fischer, C. M. Isborn, and O. V. Prezhdo, Chem. Sci. **2**, 400 (2011).

[19] X. D. Pi, J. Nanomater. **2012**, 912903 (2012).

[20] A. R. Stegner, R. N. Pereira, K. Klein, R. Lechner, R. Dietmueller, M. S. Brandt, M. Stutzmann, and H. Wiggers, Phys. Rev. Lett. **100**, 026803 (2008).

[21] X. D. Pi, R. Gresback, R. W. Liptak, S. A. Campbell, and U. Kortshagen, Appl. Phys. Lett. **92**, 123102 (2008).

[22] A. R. Stegner, R. N. Pereira, R. Lechner, K. Klein, H. Wiggers, M. Stutzmann, and M. S. Brandt, Phys. Rev. B **80**, 165326 (2009).

[23] M. Xie, D. S. Li, L. Chen, F. Wang, X. D. Zhu, and D. Yang, Appl. Phys. Lett. **102**, 123108 (2013).

[24] H. C. Sun, J. Xu, Y. Liu, W. W. Mu, W. Xu, W. Li, and K. J. Chen, Chin. Phys. Lett. **28**, 067802 (2011).

[25] A. Mimura, M. Fujii, S. Hayashi, D. Kovalev, and F. Koch, Phys. Rev. B **62**, 12625 (2000).

[26] E. G. Barbagiovanni, L. V. Goncharova, and P. J. Simpson, Phys. Rev. B **83**, 035112 (2011).

[27] K. Seino, F. Bechstedt, and P. Kroll, Nanotechnology **20**, 135702 (2009).

[28] M. Luppi and S. Ossicini, Phys. Status Solidi A **197**, 251 (2003).

[29] Z. Y. Ni, X. D. Pi, and D. Yang, RSC Adv. **2**, 11227 (2012).

[30] J. Xu, W. w. Mu, Z. Y. Xia, H. C. Sun, D. Y. Wei, W. Li, Z. Y. Ma, and K. J. Chen, J. Non-Cryst. Solid. **358**, 2141 (2012).

[31] Z. H. He, J. Xu, W. Li, K. J. Chen, and D. Feng, J. Non-Cryst. Solid. **266**, 1025 (2000).

[32] A. Carvalho, M. J. Rayson, and P. R. Briddon, J. Phys. Chem. C **116**, 8243 (2012).

[33] X. D. Pi, X. B. Chen, and D. Yang, J. Phys. Chem. C **115**, 9838 (2011).

[34] E. Holzenkämpfer, F. W. Richter, J. Stuke, and U. Voget-Grote, J. Non-Cryst. Solid. **32**, 327 (1979).

[35] D. L. Griscom, E. J. Friebele, K. J. Long, and J. W. Fleming, J. Appl. Phys. **54**, 3743 (1983).

[36] R. A. Weeks, J. Non-Cryst. Solid. **179**, 1 (1994).

[37] A. Stirling and A. Pasquarello, Phys. Rev. B **66**, 245201 (2002).

[38] K. Seino, F. Bechstedt, and P. Kroll, Phys. Rev. B **82**, 085320 (2010).

[39] B. Delley, J. Chem. Phys. **92**, 508 (1990).

[40] B. Delley, J. Chem. Phys. **113**, 7756 (2000).

[41] E. Degoli, G. Cantele, E. Luppi, R. Magri, D. Ninno, O. Bisi, and S. Ossicini, Phys. Rev. B **69**, 155411 (2004).

[42] M. Lopez del Puerto, M. Jain, and J. R. Chelikowsky, Phys. Rev. B **81**, 035309 (2010).

[43] C. Delerue, M. Lannoo, and G. Allan, Phys. Rev. Lett. **84**, 2457 (2000).

[44] A. J. Williamson, J. C. Grossman, R. Q. Hood, A. Puzder, and G. Galli, Phys. Rev. Lett. **89**, 196803 (2002).

[45] A. Puzder, A. J. Williamson, F. A. Reboredo, and G. Galli, Phys. Rev. Lett. **91**, 157405 (2003).

[46] A. Puzder, A. J. Williamson, J. C. Grossman, and G. Galli, J. Am. Chem. Soc. **125**, 2786 (2003).

[47] R. Wang, X. D. Pi, and D. Yang, J. Phys. Chem. C **116**, 19434 (2012).

[48] I. Vasiliev, S. Öğüt, and J. R. Chelikowsky, Phys. Rev. Lett. **86**, 1813 (2001).

[49] I. Vasiliev, S. Öğüt, and J. R. Chelikowsky, Phys. Rev. B **65**, 115416 (2002).

[50] C. S. Garoufalis, A. D. Zdetsis, and S. Grimme, Phys. Rev. Lett. **87**, 276402 (2001).

[51] Q. S. Li, R. Q. Zhang, S. T. Lee, T. A. Niehaus, and T. Frauenheim, J. Chem. Phys. **128**, 244714 (2008).

[52] Q. S. Li, R. Q. Zhang, S. T. Lee, T. A. Niehaus, and T. Frauenheim, Appl. Phys. Lett. **92**, 053107 (2008).

[53] X. B. Chen, X. D. Pi, and D. Yang, Appl. Phys. Lett. **99**, 193108 (2011).

[54] X. B. Chen, X. D. Pi, and D. Yang, J. Phys. Chem. C **115**, 661 (2011).

[55] C. Delerue, G. Allan, and M. Lannoo, Phys. Rev. B **48**, 11024 (1993).

[56] D. L. Dexter, in *Solid State Physics, Advances in Research and Applications*, edited by F. Seitz and D. Turnbull (Academic, New York, 1958), Vol. 6, p. 360.

[57] M. Lannoo, C. Delerue, and G. Allan Phys. Rev. Lett. **74**, 3415 (1995).

[58] G. Cantele, E. Degoli, E. Luppi, R. Magri, D. Ninno, G. Iadonisi, and S. Ossicini, Phys. Rev. B **72**, 113303 (2005).

[59] L. G. Wang and A. Zunger, Phys. Rev. B **66**, 161202 (2002).

[60] T. L. Cottrell, *The Strengths of Chemical Bonds*, 2nd ed. (Butterworths Scientific Publications, London, 1958).

[61] N. Fukata, S. Ishida, S. Yokono, R. Takiguchi, J. Chen, T. Sekiguchi, and K. Murakami, Nano Lett. **11**, 651 (2011).

[62] S. Kim, J. S. Park, and K. J. Chang, Nano Lett. **12**, 5068 (2012).

[63] K. Sakamoto, K. Nishi, F. Ichikawa, and S. Ushio, J. Appl. Phys. **61**, 1553 (1987).

[64] Y. S.Kim and K.Chang, J. Appl. Phys. Lett. **87**, 041903 (2005).

[65] D. V. Melnikov and J. R. Chelikowsky, Phys. Rev. Lett. **92**, 046802 (2004).

[66] S. Zeng, G. N. Aliev, D. Wolverson, J. J. Davies, S. J. Bingham, D. A. Abdulmalik, P. G. Coleman, T. Wang, and P. J. Parbrook, Appl. Phys. Lett. **89**, 022107 (2006).

[67] X. Wang, R. Q. Zhang, S. T. Lee, Th. Frauenheim, and T. A. Niehaus, Appl. Phys. Lett. **93**, 243120 (2008).